Types of Optical Coherence Tomography for Cancer Diagnosis: A Systematic Review

Neha Acharya[1], Sindhoora K. Melanthota[1], Manoj Khokhar[2], Shweta Chakrabarti[3], Dharshini Gopal[3], Dhyeya S. Mallya[1], and Nirmal Mazumder[1*]

[1] Department of Biophysics, Manipal School of Life Sciences, Manipal Academy of Higher Education, Manipal, Karnataka 576104, India

[2] Department of Biochemistry, All India Institute of Medical Sciences, Jodhpur, Rajasthan 342005, India

[3] Department of Bioinformatics, Manipal School of Life Sciences, Manipal Academy of Higher Education, Manipal, Karnataka 576104, India

*** e-mail:** nirmaluva@gmail.com

Abstract. Optical coherence tomography (OCT) is an emerging imaging technique that produces high contrast images that help distinguish different tissue layers by detecting the back-reflected near-infrared light. The technique is used to diagnose various diseases due to high contrast, three-dimensional imaging capability with high resolution, and a fast acquisition speed. The meta-analysis study was performed by the systematic review of literature in PubMed, Web of Science, Scopus, Google Scholar, Embase, and Cochrane Library using search terms relevant to "OCT", "Carcinoma", and "cancers". The various applications of different types of OCT are discussed in the detection and diagnosis of various cancers like colorectal cancer, breast cancer, skin cancer, brain cancer, prostate cancer, ovarian cancer and lung cancer. © 2022 Journal of Biomedical Photonics & Engineering.

Keywords: optical coherence tomography; cancer; tissue imaging.

Paper #3440 received 28 Jun 2021; revised manuscript received 01 Dec 2021; accepted for publication 21 Dec 2021; published online 4 Feb 2022. doi: 10.18287/JBPE22.08.010201.

1 Introduction

Optical coherence tomography (OCT) is a non-invasive, label-free optical imaging technique used for obtaining high-resolution images of biological tissues and other objects in real-time [1]. It was initially reported in 1991 as having a similar working principle as ultrasonic imaging where the reflected sound waves are detected, but OCT detects a back-reflected near-infrared light source (wavelength range of 700–1300 nm) [2, 3]. The resolution, however, is 10–50 times greater than ultrasound. Since OCT uses a longer wavelength, it can image at high resolution (2 to 15 μm), and profound imaging depth of up to 2 mm as scattering decreases with an increase in wavelength. OCT is used in imaging highly scattering tissues, where backscattered light is selected interferometrically from a defined depth, allowing two- and three-dimensional imaging wherein the source of endogenous contrast used is the local backscattering coefficient [4]. It is applied to the living cortex for refractive index measurements when a transmission measurement is infeasible. The light scattering ability of several tissues is responsible for the contrast generated. The technique is regarded as non-invasive imaging, having both *in vivo* and *ex vivo* applications. Optical fibre-based OCT can be combined with a great variety of instruments such as laparoscopes, endoscopes, catheters and surgical probes for real-time internal site imaging [5]. It is also a propitious technique for guidance during the abscission of tumours. The reflectance at the boundaries between multiple structural layers is measured within the sample. OCT is a non-contact optical helpful technique in imaging organs that cannot be biopsied, like the retina. The reflection delay of the targeted waves is calculated to obtain the depth of reflection. The dislocation of the beam is measured to obtain the cross-sectional image (tomography). Since the measurement of the delay in the reflection is tricky, a reference of measurement is utilized where one part of the light is given to sample and another to a reference with a known length [6]. Hence, it can provide information about the internal structure of the tissues and organs within seconds as it has a higher image acquisition speed. The speed is usually determined based on the rate

at which the depth of tissue is scanned per second, which is referred to as A-scans [7]. Therefore, the technique is used in various biomedical applications, including ophthalmology, dermatology, cardiology, cancer, neuroscience, dentistry, etc. [1]. In this review, we discuss the various types of OCT in the diagnosis of cancers associated with colon, skin, breast, brain, ovary, prostate and lungs.

2 Methodology

With a simple search of the MEDLINE database in PubMed, we have found a large number of literature on various applications of OCT in the field mentioned above. The graphical representation of the collection of publications in the last 10 years with search items as "type of technique" and "application" is illustrated (Fig. 1). Since most of the publications are in the field of ophthalmology, followed by cancer, cardiology, and neuroscience, there is tremendous room for further research in cancer.

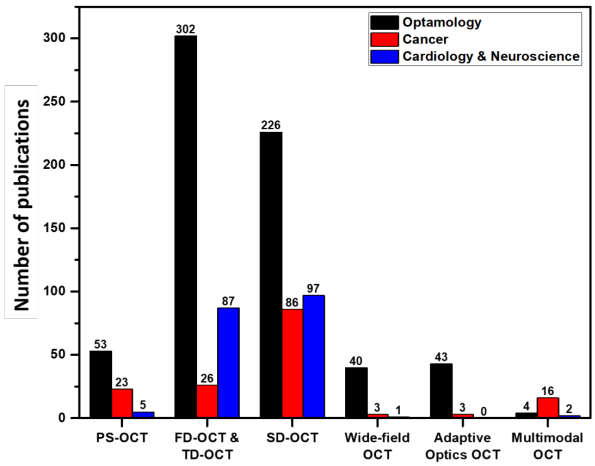

Fig. 1 The total number of publications in PubMed on applications for various types of OCT in last 10 years.

2.1 Search Strategy

Since no ethical regulation was required for meta-analysis studies, we searched electronic databases such as PubMed, Web of Science, Scopus, Google Scholar, Embase and Cochrane Library for the last 10 years, i.e., 2010 to 2020. The search queries used include "Optical coherence tomography and cancer or carcinoma", "Optical coherence tomography and Prostate cancer or carcinoma", "Optical coherence tomography and lung cancer or carcinoma", "Optical coherence tomography and skin cancer or carcinoma", "Optical coherence tomography and colorectal cancer or carcinoma", "Optical coherence tomography and ovarian cancer or carcinoma", "Optical coherence tomography and breast cancer or carcinoma", and "Optical coherence tomography and brain cancer or carcinoma". A total of 1018 papers was identified. Reviewing of papers were performed by two reviewers, and a third reviewer solved any conflicts.

2.2 Inclusion and Exclusion Criteria

The criteria applied to include the studies for the meta-analysis were as follows: (i) studies including the application of OCT to detect and diagnose cancer or malignant cells or tissues, (ii) articles from which adequate data could be extracted such as true and false negatives and true and false positives values, and (iii) relevant articles published in the past decade (2010 – 2020). The criteria based on which papers were excluded as follows: (i) reviews, animal studies, book chapters, and conference proceedings, (ii) articles for which abstracts were not available, (iii) papers where OCT was not used for the diagnosis of cancer, (iv) papers in other languages except English, (v) articles including OCT for retinal imaging, and (vi) studies without any sufficient data. With inclusion and exclusion criteria, 36 papers are shortlisted in this review. Table 1 summarizes the types of optical coherence tomography for the diagnosis of different cancers, Table 2 compares different types of OCT for cancer diagnosis, and Table 3 provides the diagnostic summary of each paper groped by various cancer type.

3 Instrumentation

The OCT has shown remarkable outcomes in detecting changes in pathology of stratified tissues such as the eye. There are various types of OCT developed to visualize the tissue structure. Fig. 2 describes various types of OCT in investigating types of cancer. Tissue-specific contrast can be generated by changing the input polarization state of light in polarization sensitive OCT (PS-OCT) [8]. Another variant of PS-OCT is cross-polarization OCT (CP-OCT), wherein parallel and orthogonal images are acquired by imaging the variations in the initial polarization caused by cross-scattering and birefringence in the tissues [9]. OCT-based angiography (OCTA) is also an OCT adjunct for non-invasive angiography, where circulation in functional vessels are envisioned without any exogenous contrast agents. In time-domain OCT (TD-OCT), the first-ever OCT, the light was divided into two beams – the central beam and the reference beam, as mentioned previously. For each depth profile (A-scan), the reference length was altered to that depth, and the combined light intensity was measured, and the sample reflectance profile is obtained. The path-length must be similar for the light from each path to interfere. The image of the cross-section is obtained by scanning the sample laterally (B-scan). Fourier-domain OCT (FD-OCT) is another type of OCT that directly encrypts the delayed time echoes in spectral interferogram. In FD-OCT, the A-scans are obtained from the spectral information present [10]. The availability of additional spectral information ensuring mechanical scanning is not necessary, unlike TD-OCT. It is classified into two forms based on configurations of the system – spectral-domain OCT (SD-OCT) and swept-source OCT (SS-OCT). SD-OCT is designed with a broad bandwidth light source, one-dimensional linear

Table 1 Types of optical coherence tomography for the diagnosis of different cancers.

Author	Year	Country	Design	Type of OCT	Type of Cancer	Number of Patients	Age (mean or median)
Li et al. [13]	2019	USA	Multimodal	Co registered OCT with near infrared (NIR) fluorescence imaging	Colorectal	NA	NA
Ashok et al. [14]	2013	UK	Multimodal	Multimodal Fourier Domain (FD) OCT with Raman spectroscopy	Colonic adenocarcinoma	66	NA
Yuan et al. [18]	2010	USA	Multimodal	Co-registered OCT and fluorescence molecular imaging (FMI) system	Colon	4	NA
Erickson-Bhatt et al. [20]	2015	Illinois	Surgical probe	Handheld surgical OCT imaging probe	Breast	35	NA
Kennedy et al. [25]	2015	Australia	NA	Needle-based OCT	Breast	1	70
Gubarkova et al. [26]	2019	Russia	Multimodal	Spectral domain (SD) multimodal OCT	Breast	33	30–80
Yang et al. [27]	2020	China	Pro	Full-field (FF) OCT	Breast	158	NA
Wang et al. [28]	2018	USA	NA	Polarization-sensitive (PS) OCT	Breast	9	NA
Butola et al. [29]	2019	India	NA	Swept-source (SS) OCT	Breast	22	NA
Zhou et al. [30]	2010	USA	Integrated	OCT and optical coherence microscopy (OCM)	Breast	44	NA
Dubey et al. [31]	2019	India	NA	OCT	Breast	24	NA
Lindner et al. [32]	2012	Germany	Pro	OCT	Breast	34	29–68
Assayag et al. [49]	2014	France	NA	FF-OCT	Breast	22	58 (mean)
Mogensen et al. [33]	2009	Denmark	NA	OCT and PS-OCT	Skin	100	NA
Adabi et al. [34]	2017	USA	NA	OCT	Skin	21	NA

Batz et al. [35]	2018	Germany	NA	OCT	Skin	25	69 (mean)
Turani et al. [36]	2019	Brazil	NA	SS-OCT	Skin	69	20–80
Tes et al. [37]	2018	USA	NA	SS-FD OCT	Skin	1	25
Coleman et al. [40]	2013	UK	NA	OCT	Skin	78	59 ± 13
Banzhaf et al. [41]	2014	Denmark	Pro	OCT	Skin	16	52–82
Ulrich et al. [42]	2015	UK	Pro	OCT	Skin	155	≥18
Marvdashti et al. [43]	2016	USA	NA	PS-OCT	Skin	42	NA
Holmes et al. [44]	2018	Germany	Pro	OCT	Skin	NA	≥18
Braunmühl et al. [45]	2016	Germany	NA	Frequency domain (FD) OCT	Skin	32	68 (mean)
Wessels et al. [71]	2015	Netherlands	NA	OCT	Skin	18	47–88
Yashin et al. [52]	2019	Russia	NA	Cross-polarization (CP) OCT	Brain	30	NA
Assayag et al. [53]	2013	France	Pro	FF-time domain (TD) – SD-OCT	Brain	18	19–81
Kut et al. [54]	2015	USA	NA	SS-OCT	Brain	37	NA
Yashin et al. [55]	2019	Russia	NA	CP-OCT	Brain	17	NA
Wang et al. [58]	2013	USA	NA	FD-PS OCT	Ovarian	18	NA
Yang et al. [59]	2012	USA	NA	PS-OCT	Ovarian	18	61
Swaan et al. [63]	2018	Netherlands	Pro	Needle-based	Prostate	4	≥18
Muller et al. [64]	2018	Netherlands	Pro	Needle-based	Prostate	20	≥18
Gardecki et al. [65]	2019	Boston	NA	Micro	Prostate	11	NA
Lopater et al. [66]	2016	France	NA	FF-OCT	Prostate	38	NA
Wei et al. [72]	2012	China	NA	FD-OCT	Lung	48	≥18

Hariri et al. [73]	2019	United States	Retro	PS-OCT	Lung	26	≥18

NA: Not applicable

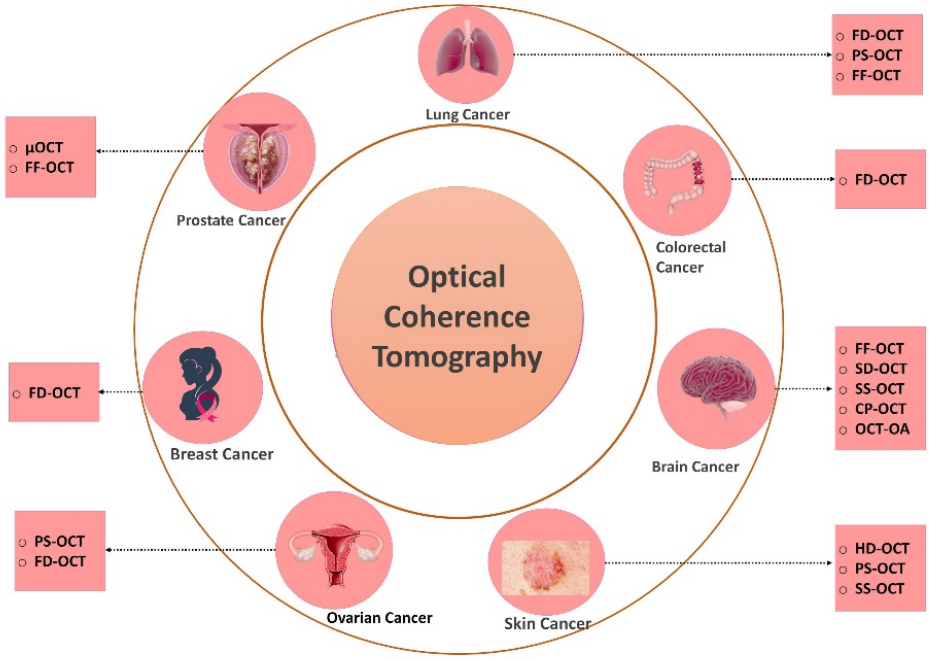

Fig. 2 Different types of optical coherence Tomography (OCT) techniques used in the diagnosis and medical treatment of various types of cancers. (Polarization-sensitive OCT (PS-OCT; cross-polarization OCT (CP-OCT); OCT-based angiography (OCTA); time-domain OCT (TD-OCT); Fourier-domain OCT (FD-OCT); spectral-domain OCT (SD-OCT); swept-source OCT (SS-OCT); Full-field OCT (FF-OCT); micro-optical coherence tomography (μOCT)).

array sensor and a spectrometer that captures the interferogram encrypting the echoes in wavelength. The spectral interferogram is captured using a single detector in SS-OCT, where the laser source frequency is swept through a range of optical frequencies [11]. FD-OCT is more sensitive than TD-OCT due to the high scanning speed and signal-to-noise ratio. The lower speed of TD-OCT is due to the reference mirror that is in motion and its cycle time, whereas in FD-OCT, it is stagnant, and multiple points can be sampled at once [12]. Full-field OCT (FF-OCT) is a recently developed method that allows a high-resolution wide-field view over the entire field and is used in cancer diagnostics [9]. A light-emitting diode (LED) or halogen is used as a light source to illuminate a full field. FF-OCT provides the 3D resolution on tissue samples that are label-free (up to a depth of 200–300 μm). The image acquisition time is less than 5 min, and imaging performance is almost the same in fresh or fixed tissue. Short pulse lasers like Cr^{4+}: Forsterite lasers are used in OCT imaging for research studies. They have a very high resolution due to their short coherence lengths and more extraordinary output powers. Cr^{4+}: Forsterite laser generates output powers of 100 mW giving pulses of 1300 nm wavelength resulting in a resolution of 5–10 μm. Ti: AI2O3 laser, another short-pulse laser, can provide resolutions of 1 μm at 800 nm. Semiconductor-based light sources or superluminescent diodes are used instead of short pulse lasers. They can have resolutions up to 15 μm and power of 10–15 mW at 1300 nm. In the following section, the applications of OCT are discussed in selected types of cancer (Fig. 3).

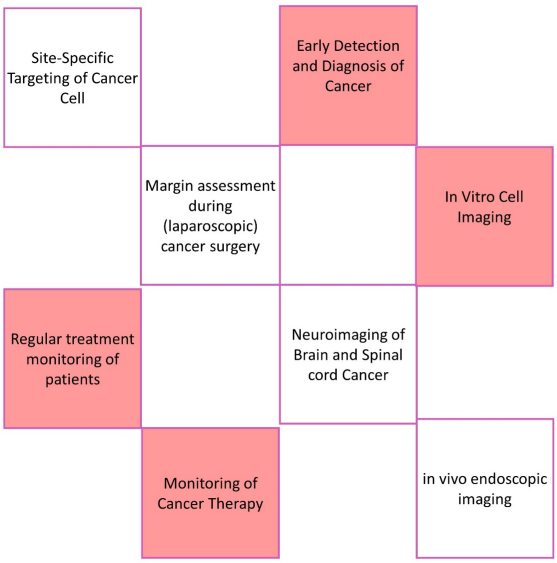

Fig. 3 The application of the OCT technique to various types of cancer.

Table 2 Compares the different types of OCT for cancer diagnosis.

Types of OCT	Principle and information	Applications	Advantages	Limitations	Cancer Type	References
Polarization sensitive (PS) OCT and cross-polarization (CP) OCT	Based on a newer contrast mechanism (backscattered light). Detects images when polarization state is orthogonal to the incident state	Intraoperative margin detection, collagen protein detection	To obtain 3-D information for analysing B-scan images and confirming the origin of the signal. Transverse resolution of ∼10 μm in the focal plane and an axial resolution of 7.6 μm in air	The rather shallow image depth that can be used to cover images and image depth is limited to ~0.5mm due high sensitivity	Lung, Skin, Breast, Ovary, Brain	[8, 9, 30]
Time-domain OCT (TD-OCT)	Based on examining the mechanical length of the path followed by light	Tumour detection	Axial resolution of 10 μm	Random property of tissue could limit its imaging resolution	Brain, Skin	[10, 12]
Fourier domain OCT (FD-OCT)	Fourier transform of the spatial correlation function of the refractive index	FD-OCT helps in understanding the structure information	Higher sensitivity due to axial locations are recorded throughout the entire A-scan duration. Resolution limit of 1–15 μm. Utilized in the clinical diagnostic screening of large tissue areas	Inadequate resolution for visualizing fine morphological details. Random property of tissue could limit its imaging resolution	Brain, Ovary, Lung, Colorectal	[10, 12, 14]
Spectral domain OCT (SD-OCT)	1-D linear array sensor, broad bandwidth light source, and a spectrometer capturing the interferogram encrypting the echoes in wavelength	Obtain tissue morphology	No pupil dilation required, higher machine speed the speed of the machines is higher, minimized motion artefacts, better image quality, and comfortable patient examination. It is used in clinical *in vivo* imaging and screening of cancer	Large file sizes and high cost. Axial resolution up to 3.8 μm	Brain	[11]
Wide-field optical coherence microscopy	Based on spectral-domain and swept-source technology	Intraoperative neurosurgical setting was demonstrated to assess tumorous glial and epileptic margins	Active eye tracking improves image stability. Spatial resolution of 1.8 μm × 0.9 μm (transverse × axial). Used for *in vivo* imaging of lesions	Lower resolution and requires artifacts minimization	Skin, Brain, Breast	[9, 20]

Multimodal OCT	OCT with a combination of ultrasound, photoacoustic/ ultrasound, near-infrared imaging (NIR), fluorescence molecular imaging (FMI) and Raman spectroscopy	Diagnostic Imaging and Treatment Monitoring	Allows cross-sectional envision of tissue morphology and vasculature with high sensitivity and spatial resolution	Limited clinical impact compared to pure OCT systems, microscopic techniques with small FOVs allow only tunnel vision in clinical diagnosis	Breast, Colorectal	[13, 14, 16, 18]

4 Applications of OCT

4.1 Colorectal cancer

Colonoscopy, considered the best technique for colorectal cancer (CRC) diagnosis, helps detect abnormal tissue growth on colon or rectum mucous membrane known as colorectal polyps. Though the technique is considered as a standard procedure, colonoscopy detects only the surface morphology of the rectal wall; also, the technique cannot determine the abnormal subsurface microvasculature, which is highly linked to CRC. Thus, a biopsy, an invasive and time-consuming method with limited accuracy, is required for cancer staging. Passing the OCT probe through the endoscope accessory channel will help the endoscope to visualise the mucosal tissue at a resolution of 2–10 μm. However, different probes have different penetration depth and resolution, and there is a need for uniformity and standardisation of endoscopic OCT techniques. To improve diagnostic accuracy, multimodal imaging systems such as OCT combined with ultrasound, photoacoustic, and near-infrared imaging (NIR) are developed. Out of these, combining OCT and NIR fluorescence is effective as it allows cross-sectional envision of tissue morphology along with the vasculature with high sensitivity and spatial resolution. The microanatomy of the structures can be visualised with much more detail with OCT, and the NIR fluorescence can help in lesion studies. Multimodality serves to improve the ability to observe the morphology and the molecular composition, and biochemistry simultaneously. Hence, it is considered an essential tool for the observation of hallmarks of colorectal cancer. Also, OCT/NIR fluorescence imaging reduces the cost of the procedure and time as data from OCT and NIR fluorescence can be acquired with a single probe in one session [13].

In a study, OCT/NIR fluorescence was combined for imaging probe into a miniature endoscope. Imaging with both components was processed simultaneously with high resolution and speed. The multimodal system was validated using food and drug administration (FDA) approved contrast agent ICG (indocyanine green) with a rat model having the CRC. The NIR fluorescence could show the changes in morphology and areas occupied by blood vessels using OCT images placed parallel (co-polarized) to each other. The tumorous region is identified due to the accumulation of ICG in a more considerable amount when compared to normal tissues hence, ICG can be used for describing the tumour border and angiogram. The amount of ICG and the distance from the probe was used to determine the signal intensity in NIR fluorescence imaging. 2D images from NIR fluorescence and corresponding OCT images placed collateral to each other indicated that polyps could be identified using 2D NIR images but not the types of polyps. Thus, for better cross-sectional visualization, OCT images were used. 3D OCT and NIR can be used for the clear identification of polyp types. Therefore, the technique is minimally invasive, and it is easier to integrate into clinical practice. Clinical studies show that the spectra obtained using fluorescence spectroscopy cannot distinguish between the cancerous tissues of the colon and non-cancerous tissues [13]. Studies showed that Raman spectroscopy was an efficient tool to distinguish between normal and cancerous tissues. However, it cannot be used as a disease diagnostic tool because the classification efficiency is very low when interpatient variability is considered [14]. Therefore, a multimodal approach where Raman spectroscopy is interfaced with methods like FD-OCT provides additional information about the tissue. Raman spectroscopy helps in understanding the biochemical nature while OCT helps in understanding the structure, information from both tools is combined to examine the capability of the multimodal system as they act as an efficient tool for non-invasive optical biopsy [15]. The study comprised normal tissue samples and tumorous samples, and images were captured using both devices for each sample [16]. A quantification algorithm must be implemented because a spectroscopic technique which is analysed numerically (quantitative) is combined with an imaging technique which is analysed categorically (qualitative), for the imaging technique. For both feature selection and parameter reduction in Raman and OCT data principle component analysis (PCA) was used.

Fig. 4 indicates that differences exist in the morphology of the two tissue types. Yet, the investigation of obtained images was insufficient for diagnosis when interpatient variability is considered. When the

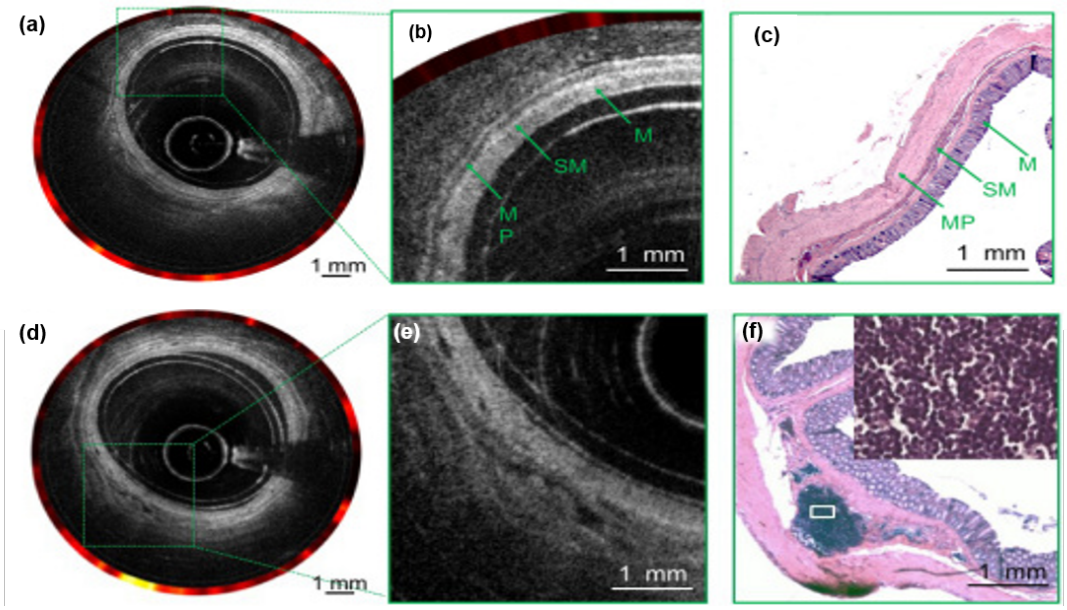

Fig. 4 (a) The combined OCT and NIR fluorescence image of normal rectum, (b) enlarged view of the dashed box in (a), (c) histology; (d) the combined OCT and NIR fluorescence image of adenocarcinoma; (e) enlarged view of the dashed box in (d); (f) histology. M: mucosa; SM: submucosa; MP: muscularis propria. Adapted with permission from [13] © The Optical Society.

multimodal approach was used in the analysis, both specificity and sensitivity were increased significantly. Though histology and excisional biopsy based on white light are considered as the standard for the detection of cancer in the gastrointestinal tract (GI), the chances of obtaining negative results are more because of sampling errors [17]. FD-OCT imaging system utilized a light source emitting with a broad spectral range. The images obtained from OCT combined with FLOT (Fluorescence-based Laminar Optical Tomography) distinguish between cancerous lesions and non-cancerous. This information was used as a criterion to estimate the dimensions of tumours, and it was observed that FLOT gives a more accurate estimation of the diameter of the tumour. In contrast, the thickness of the tumour was determined from OCT images when placed orthogonally [18].

4.2 Breast cancer

Breast-conserving surgery (BCS) is a method used to treat early-stage breast cancer, which when followed by radiotherapy shows lower mortality over mastectomy [19]. Thus, the necessity of identification and complete resection of the tumour has been increased significantly. Since all these methods are time-consuming and have high sampling errors, developing a technique that allows live imaging and detection of tumour margins is crucial. Among different methods developed, OCT was a very effective tool for intraoperative margin assessment of breast tumour [20, 21]. Explicitly, it is observed that scattering was more in the case of breast cancer samples when compared to non-cancerous tissues. Thus, it is possible to distinguish the cancerous and healthy tissues. A portable intraoperative SD-OCT system, where image contrast was based on backscattered light (polarization-sensitive) was developed [20]. Human subjects undergoing reduction mammoplasty (breast reduction surgery) or mastectomy were recruited for the study. Correlation coefficient analysis was performed to classify the closely correlated images based on their location. The adipocytes were recognizable due to their shape and lipid content in the OCT image of the tissue, which shows that conventional OCT on itself can distinguish between the fibro-adipose tissue and Invasive Ductal Carcinoma (IDC). Tumour cells and the healthy breast tissue in IDC result in disruption of the collagen structure, which is less delayed compared to the normal stroma. Significant differences between stroma and IDC were observed from delayed (retardation), and Degree of Polarization Uniformity (DOPU) derived OCT analysis based on backscattered light. The measurements use metrics, CV, DOPU and retardation the capacity of the OCT to diagnose the disease was assessed.

Breast cancer is a collective disease that exhibits a wide range of clinical, structural and molecular attributes among tumours and within a tumour. Breast cancer is classified into non-invasive (Ductal cancer in situ- DCIS) and invasive types (Luminal A, Luminal B, HER2-positive) and basal-like (triple-negative) subtypes [22]. The study of structural and molecular breast cancer features helps in detection of tumour margin vividly. Imaging methods of breast cancer such as X-ray computed tomography, ultrasound, positron emission tomography (PET), and magnetic resonance imaging (MRI) are used to determine the dimension of tumour or lymph node, the general structural information or morphology [23], however, tissue having less than a few

mm and false (negative) surgical margin cannot be determined using these methods due to the low resolution. To overcome this, a technique with a high optical resolution which can approach the histopathology level in providing details in nearly real-time to detect the margins of lumpectomy. The conventional OCT images do not provide information about the rigidity of the tissue, hence Optical Coherence of Elastography (OCE) images of the reference tissue can be compared with the deformed states tissue to obtain such information [24, 25]. The study shows that the OCE-based approach can assess the morphology, malignancy degree of tumours, and categorization of cancer subtypes. Samples of freshly resected breast tissues obtained from patients were used. The specimens included both the tumorous region and peritumoral area and were studied within a short duration of time after the resection. The samples were categorized into benign and malignant breast tissues based on the histopathology results. Real-time polarization-sensitive images of the tissue are obtained using a customized multimodal SD-OCT system. The images were used to detect the state of connective tissue component when the OCT images are placed orthogonally (cross-polarized). The OCT-based findings were compared with results of the histopathology. The results indicated the differences between various types of tissues [25]. OCE images in Fig. 5 showed the details of the ducts filled with tumour cells for breast cancer Ductal Carcinoma in Situ (DCIS) and Luminal A with highly increased stiffness. Thus, the technique can be used to distinguish the different cancer subtypes. Also, the images obtained showed a higher contrast than the images obtained from standard and PS-OCT images [26].

Normal, cancerous tissues, benign breast lesions, and resected axillary lymph nodes were examined using FF-OCT. The minimum sensitivity and high specificity were observed in breast cancer diagnosis, and they diverged in nodal assessments. These tissue-sparing approaches proved highly efficient in breast cancer and nodal metastasis diagnosis compared to histology [27]. The implementation of PS-OCT for enhancing breast cancer detection was reported. The standard OCT and PS-OCT-based metrics obtained were complementary for the differentiation of healthy fibro-adipose tissue, stroma, and IDC, differentiated with an accuracy of 89.4%, illustrating the potential of PS-OCT for intraoperative differentiation of human breast cancer [28]. A machine learning (ML) algorithm performed the volumetric analysis of normal and breast cancer tissue and their classification based on a support vector machine (SVM) by the SS-OCT images. This algorithm classifies the cancerous tissue with 91.56% sensitivity, 93.86% specificity, and 92.71% accuracy and extracts features from the whole volume of the tissue. Therefore, breast cancer diagnosis by extracting quantitative features from various types of OCT images could be a potential approach and a key tool for a fine-needle-guided biopsy [29].

The entire tumour, along with the surrounding healthy tissue is removed using breast-conserving surgery (BCS). Tumour margins are assessed based on histopathological analysis. It is found to be a not so efficient tool that leads to the re-excision to remove additional tissue, hence tools enabling effective removal of tumorous tissue is used to reduce re-excision rates. Despite several advantages, conventional OCT cannot differentiate tumour from uninvolved stroma [29–31]. Hence, OCT integrated with OCE is used to measure the tissue deformation, and an image of tissue elasticity is acquired. Optical coherence micro-elastography (OCME) is a type of OCE capable of detecting the difference in phase and compressibility of tissue. It was found to clearly distinguish between a malignant tumour and uninvolved stroma resected human breast tissue. For tissues with dimensions of ~50 × 50 mm, a wide-field imaging system is used.

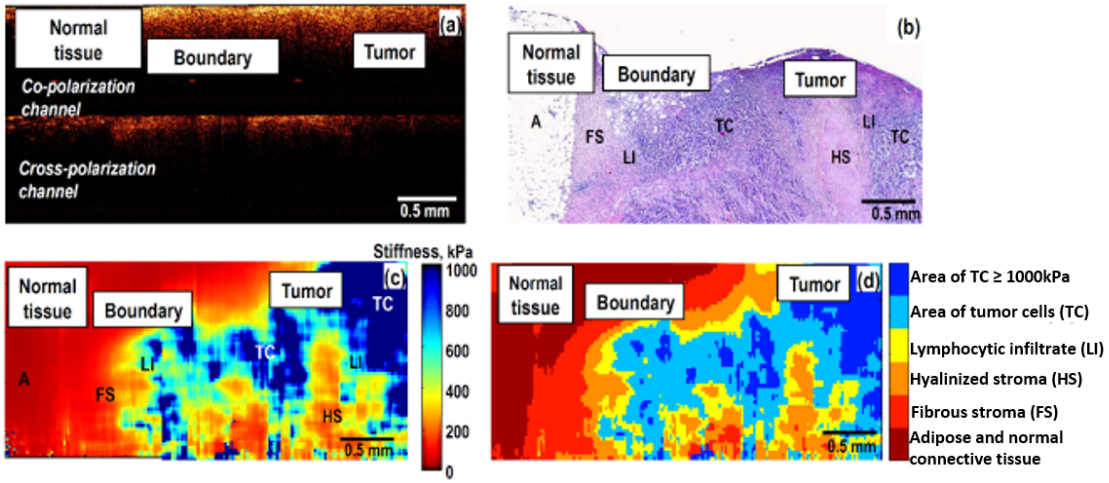

Fig. 5 Visualization of a transitional zone between normal breast tissue and tumour region with (a) the CP OCT image; (b) H&E-histological slice; (c) stiffness map; (d) morphological segmentation of the OCE image into areas corresponding to various tissue components. Adapted with permission from [26] © The Optical Society.

The study based on an FD-OCT system-generated OCT images by creating a network of images to image a larger area. The results showed wide-field elastograms had strain only in denser tissues. OCT images and elastograms obtained from patients undergoing either mastectomy or BCS are used. In both the benign tumour images, papilloma appeared to have a highly fibrous structure, while the orientation of the fibres appeared to be more organized in malignant tumours [26]. Images were obtained from a dissected tumour and a lumpectomy also. Thus, it was observed that the wide-field OCME could be used as a tool to assess the margins of resected breast tissue. Features extracted from OCT images are used to classify normal, and cancer breast tissues with the help of a multi-level ensemble model. The measurement can be used as a biomarker for removal of whole tumour tissue without any special tissue preparation [31]. Evaluation of hair shaft alterations using OCT in chemotherapy-induced alopecia was performed by Lindner et al. [32]. After chemotherapy, significant changes were observed in hair structure may be due to reduction of hair shaft calibre which could be studied by OCT imaging to gain more insight into induced changes [32]. The ability of OCT is to allow surgeons observe the morphological characteristics of the tissues, at a greater surface area also while ensuring the tissue is not damaged makes it an attractive tool in studying breast cancer [5].

4.3 Skin cancer

Studies reveal that OCT can be used for the detection of skin cancer because of its ability to envision features beneath the dermal layers, which are prominent areas for the initial appearance of skin cancer. It is found that the collagen alignment and distribution are altered due to the development of skin cancer which results in a change in the optical anisotropic nature (birefringence) of skin [31, 32]. Differentiation of different skin cancer types using OCT imaging was evaluated, and correlations between various tumour types and recurring tumour characteristics were observed [33]. The basal cell carcinoma (BCC) is commonly observed in Caucasians [34]. The disease is found to be multifactorial, and excess exposure to the sun plays a significant pathogenic role. Clinical diagnosis of BCC is usually performed using dermoscopy [35]. Non-invasive techniques such as reflectance confocal microscopy (RCM) [36], conventional OCT and multiphoton tomography (MPT) are also available for *in vivo* diagnosis. High-definition optical coherence tomography (HD-OCT) is a technique that helps in a non-invasive diagnosis with real-time 3D imaging capability and at a cellular resolution. A pilot study including HD-OCT images of superficial BCC, nodular BCC and infiltrative BCC was conducted and the lesions were fully excised and examined histopathologically for confirmation. This technique could distinguish between the subtypes, and further development in the technique could explore the skin up to micrometre level depth [37, 38].

BCC lesions depth can be determined using OCT. An OCT signal of low strength at the periphery of the cell nests was identified as corresponding to cellular palisading. The optical attenuation coefficient on OCT and the nuclear-cytoplasmic ratio of cells from histology were correlated with weak inverse linearity. OCT provides accurate measurement of BCC, along with identifying the presence of peripheral palisading [39, 40]. Banzhaf et al. [41] reported the lesions studied BCC imaging using OCT throughout imiquimod treatment in 20 biopsy-verified patients were identified both clinically and using OCT. It was observed that OCT identified all the lesions. The quality of the images was reduced due to crusting, ulceration and active treatment. OCT showed thinning of acute keratosis (AK), indicating the treatment effect. All treated BCCs were cleared, but residual tissues in 4 cases were observed clinically, this could be ruled out by OCT. OCT imaging along with clinical evaluation and dermoscopy improved the diagnostic accuracy of BCC from 65.8% to 87.4% [42]. Extraction of features such as intensity and phase retardation from polarization-sensitive OCT (PS-OCT) images for the classification of normal and cancer tissues was reported by Marvdashti et al. [43] achieved 95.4% sensitivity and specificity in detecting BCC. In another study, the impact of diagnostic parameters such as image quality, lesions, observer and inter observer variability on the diagnostic performance of OCT for the assessment of diagnostic potency of BCC subtypes in 234 patients was studied. It was observed that lesion location had no impact on OCT diagnostic performance, whereas the image quality, observer confidence had a direct correlation. Overall, BCC subtype could be determined with moderate accuracy [44]. FD-OCT imaging was used to extract and evaluate morphological features of BCC with horizontal and vertical imaging modes, which provides information required for the diagnosis, especially in nodular BCC [45].

Granular cell tumour (GCT), also called Abrikossoff tumour, is a rare soft tissue neoplasm that is usually benign. The occurrence is more in women and dark-skinned individuals and less in children. It is mainly known to occur in the oral cavity, and malignancy is less (1–2%). Surgical excision is the only treatment of GCT. Therefore, a technique that accurately evaluates the morphology and extension of the tumour is required [46]. SS-OCT system was used with a high-speed tuneable laser source. An axial scan (A-scan) obtained from the reflectivity profile was grouped for different transversal positions to generate a cross-sectional image and is referred to as B-scan. The object's top view was depicted in the C-scan. The results demonstrated that the OCT images of GCT show verrucous epidermal hyperplasia, which appears as the hyperreflective, uneven surface of the tissue. Also, the dermo-epidermal junction is visible in the healthy skin but is not distinct in the GCT region. Thus, the abnormal skin can be delineated using this technique to differentiate healthy tissue from tumorous tissue.

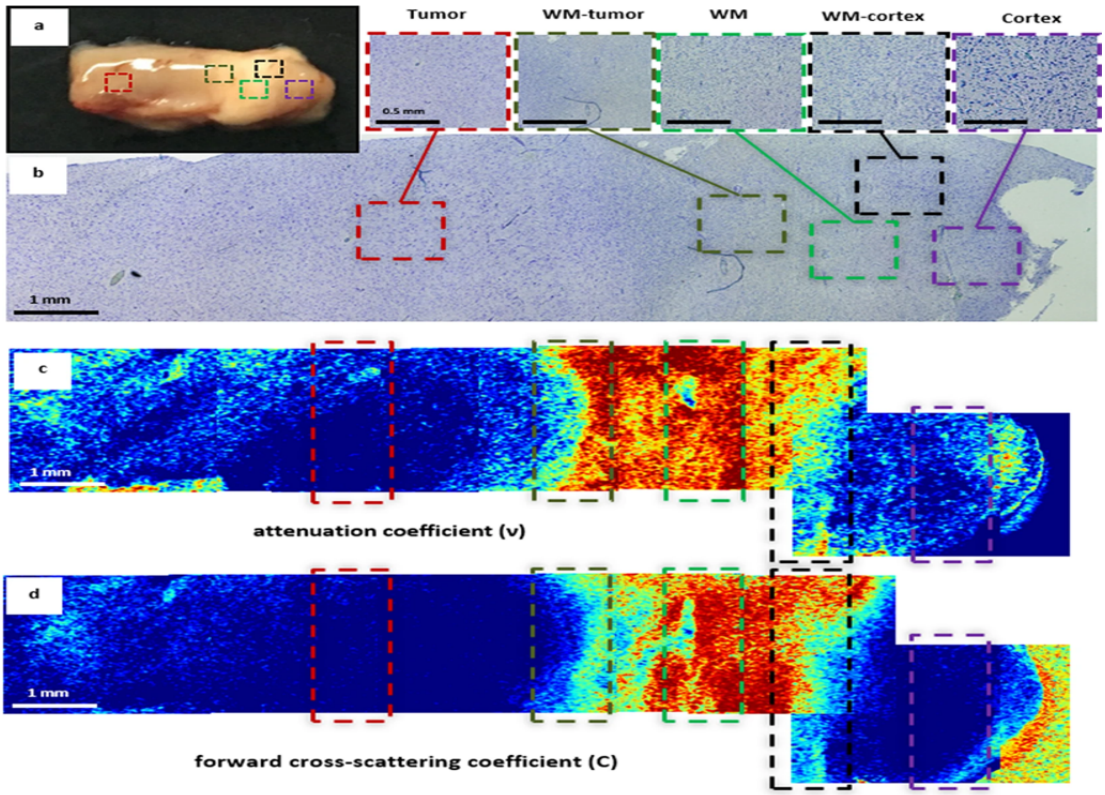

Fig. 6 (a) Brain specimen marked with different areas of interest by different colours; (b) with corresponding histology; (c) colour-coded maps based on attenuation coefficients; (d) colour-coded maps based on forward cross-scattering coefficients. WM-white matter. The Figure is adapted with kind permission from [52].

4.4 Brain cancer

Brain cancer patients have finite survival time as it recurs and later leads to death. Surgery is considered the only best treatment. The extent of resection is a significant risk factor linked to delayed tumour reappearance and, thus, longevity of the patient [46, 47]. Tissues from patients with grade II, grade IV brain cancers were obtained from surgery navigated by MRI and SS-OCT cross-sectional images. The precise identification of high-grade and low-grade human brain cancer was performed based on the established attenuation threshold. Microscopic structures that add to attenuation data in categorizing cancer from non-cancer white matter were identified using OCT images. High-grade cancer appeared as heterogeneous regions in which hyper-intense signals surrounded hypo-intense signals. Thus, OCT images enabled the identification of necrosis and hyper-cellularity [47].

A collection of tumours, including benign, malignant and slow-growing, are observed in the primary central nervous system (CNS). Patients with brain tumour survive only on complete resection of tumour mass, which is identified through postoperative imaging. Full-field OCT (FF-OCT) is a recently developed method that allows a high-resolution wide-field view [48]. A light-emitting diode (LED) or halogen is used as a light source to illuminate the full field. FF-OCT provides the highest OCT 3D resolution on tissue samples that are label-free (up to a depth of 200–300 μm). The image acquisition time is less than 5 min, and imaging performance is almost the same in fresh or fixed tissue [49]. Studies show that TD- or SD-OCT systems have an inadequate resolution for visualizing fine morphological details in CNS studies. The myelinated axon cell fibres, cyton of neurons and vasculature in the human epileptic brain and cerebellum were studied using the FF-OCT images. The images distinguished between meningiomas and hemangiopericytoma in meningeal tumours. The modifications in the architecture of brain tissue generated by infiltrative gliomas were detected.

Medulloblastoma is the most prominent malignant paediatric brain tumour with the highest ability to spread across the tissues (metastasize). The flow of cerebrospinal fluid is blocked due to the proliferation of the tumour, causing hydrocephalus. Surgical resection, chemotherapy and high-dose radiation are the treatment options used commonly, but most paediatric patients suffer from impaired intelligence and neurocognitive dysfunction due to the radiation treatment [9, 50]. Since it provides microstructural resolution and has an association with histology, OCT is considered a significant biomedical imaging modality for detecting brain tumours. The optical coefficient was measured for glioma specimens obtained *in vivo* and *ex vivo*. OCT optical attenuation (OCT-OA) images, as depicted in Fig. 6, have shown a significant correlation with histological images and provide enhanced distinction compared to structural OCT images using the local attenuation [51, 52].

Diagnosis of brain tumour was carried out using FF-OCT, a non-invasive technique that does not even

need contrast agent and tissue preparation. Imaging of brain tumours including low-grade and high-grade gliomas, meningiomas, and choroid plexus papilloma was performed. A neuron, CNS vasculature, and myelin fibres subpopulations were detected. Cortex could also be identified, but glial cells including astrocytes were not observed. The first application of label-free and real-time FF-OCT for brain cancer imaging was reported by Assayag et al. [53]. The feasibility of label-free, quantitative OCT for differentiating cancerous from non-cancerous human brain tissues was tested by Kut et al. [54] based on volumetric OCT imaging data. Lower optical attenuations of both cancerous core and infiltrated zones were compared with non-cancerous white matter, OCT achieved high sensitivity and specificity. This attenuation threshold was used to confirm the intraoperative feasibility, and it was observed that the OCT system displays a colour-coded map in real-time, thus providing direct visual cues for cancer versus non-cancer regions. In the study conducted by Yashin et al. [55], CP-OCT was performed on the brain to distinguish between cancerous and non-cancerous cells. CP-OCT scans were compared with the histology of specimens. The method showed 87–88% accuracy in diagnosis. *In vivo* CP-OCT images of brain tumour displayed vertical striations due to blood vessels. The distinctive feature of CP-OCT was its single intensity. The neuro-navigation feature of CP-OCT could help neurosurgeons with valuable information.

4.5 Ovarian cancer

Ovarian cancer is the form of cancer that has the highest death rates of all the gynaecologic cancers. The survivability is less due to the early metastasis and absence of effective techniques for disease screening and diagnosis [56]. Prophylactic oophorectomy (PO) is considered the standard treatment found to reduce the risk of ovarian cancer [56]. Also, new intraoperative devices that could diagnose ovarian cancer in earlier stages reduce the use of PO and decrease the high death rate, particularly in women with a higher chance of acquiring the disease [56]. OCT combined with techniques like ultrasound, photoacoustic imaging enhances optical absorption of tissue, scattering information and structures of tissues present at deeper sites. FD-OCT system for which swept source is based on the bandwidth (110 nm) was used. Ovaries from different species, both human and porcine species were used. The boundary indicating the presence of a cyst or follicle beneath and tissue features were visualized using OCT images [57].

A logistic prediction model employing the phase retardation rate, obtained from phase images of polarization-sensitive OCT (PS-OCT), as a parameter to characterize the malignant and normal ovarian tissue with 100% sensitivity and specificity was introduced, which could be an effective tool for the detection and diagnosis ovarian cancer [58]. A mathematical descriptor reducing the dimensions of a classifier's input data while preserving essential features was presented by St-Pierre et al. [57] that allowed exploring the features space leading to optimal classification. Multiple statistical models were presented with < 70% accuracy for the detection of cancer tissue. The approach reduces the resources required to achieve accurate classification, enabling intraoperative surgical guidance. The studies showed that PS-OCT is an adequate device to detect ovarian cancers, as the phase retardation and optical scattering co-efficient are obtained from benign and malignant ovaries, respectively. Sirius Red staining was also used to assess the properties. The results show that PS-OCT parameters such as phase retardation and scattering coefficients are significant in detecting ovarian cancer. The phase retardation images of normal and cancerous ovarian tissue from conventional OCT and phase retardation is given in Fig. 7. Since the phase retardation of normal and malignant express varying features, combining it with the calculated scattering coefficient is expected to be an efficient method in determining the disease [58]. These parameters extracted from ovarian samples are fed into the logistic model for training to achieve the automated classification of ovarian tissues as benign and malignant. Hence, a multiple parameter approach used for ovarian tissue characterization was more efficient [59].

4.6 Prostate Cancer

Prostate cancer is one of the most common organ cancers diagnosed in males by prostate-specific antigen (PSA) testing. Over diagnosis and treatment of the patients could be caused by PSA testing [60]. Prostate biopsy procedures are a potential source for diagnosis, however, challenges such as lack of standard isolation and purification techniques, labour-intensive, contamination risks and sampling errors may lead to misdiagnosis [61, 62]. Therefore, adapting to an alternative approach is essential to treat prostate cancer, and one such technique involves employing OCT for imaging of tissues. Swaan et al. [63] presented a study to assess the feasibility of focal imaging with confocal laser endomicroscopy (CLE) and needle-based OCT for differentiating normal and cancerous prostate tissues on both qualitative and quantitative basis, which includes visualization and analysis of tissues, tumour grade, and real-time architecture. This approach provided high-resolution imaging in real-time and characteristics of prostate cancer in association with transrectal ultrasound fusion-guided biopsy processes providing keen insight into the feasibility and of CLE and OCT for real-time analysis of prostate cancer.

Mullar et al. [64] acquired datasets of 106 needle-based 3D-OCT from 20 prostates, and the OCT images were grouped based on histology and precise matching, blind assessment of the same was carried out by two reviewers calculating the sensitivity and specificity of the detected malignancy, which was found to be significantly different based on quality. It was observed that needle-based OCT was reliable in discriminating between benign glands and regular, fat or cystic atrophy (Fig. 8). Quantitative assessment by Kruskal-Wallis test also

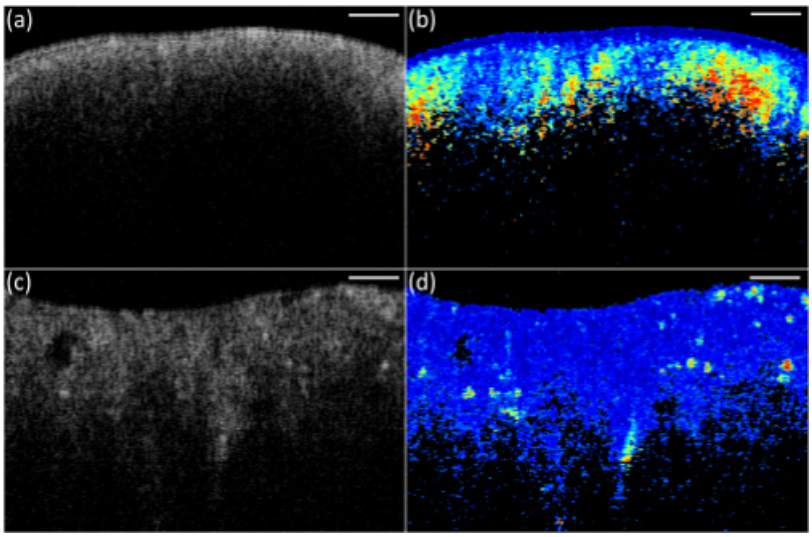

Fig. 7 (a, c) Conventional OCT and (b, d) phase retardation images from (a, b) normal and (c, d) malignant ovarian tissue. Scale bar: 0.5 mm. Adapted with permission from [59] © The Optical Society.

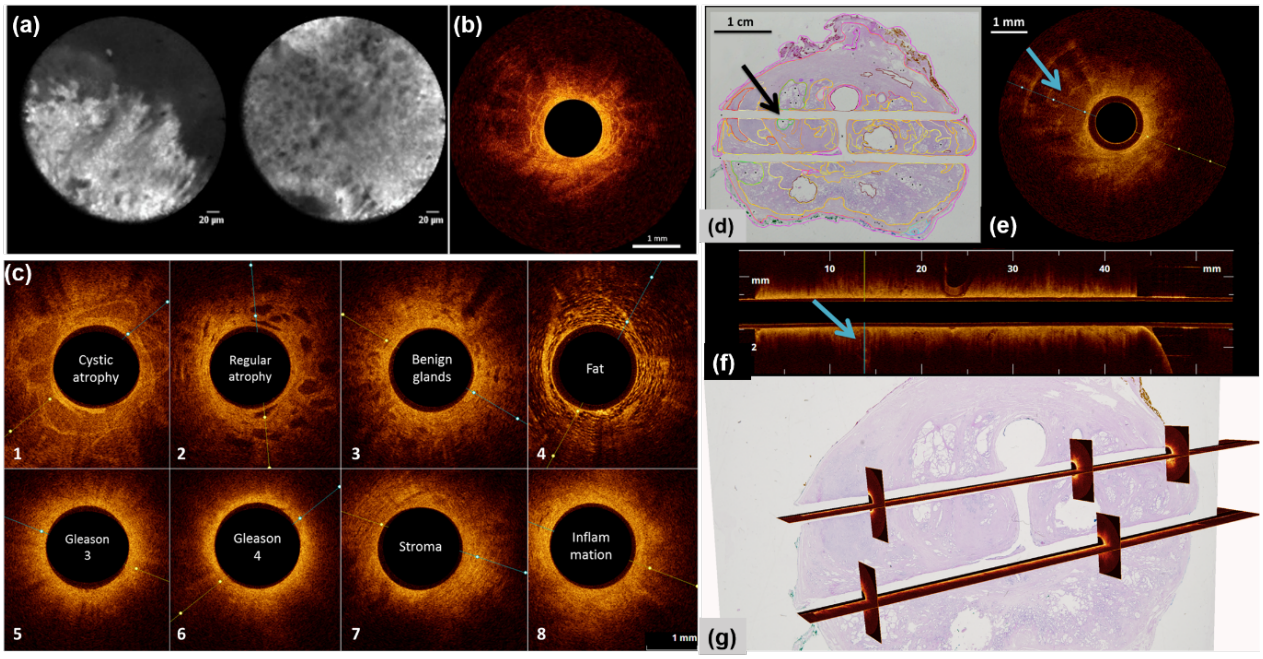

Fig. 8 (a) CLE images of *ex vivo* prostate tissue with probe soaked in fluorescein solution, (b) OCT image of the fixated *ex vivo* prostate tissue, (c) histological features seen in the OCT images, (d-g) correlation of OCT and histology where (d) depicts the tissue types in different colours indicating atrophic cyst by a black arrow, (e) OCT scan of the atrophic cyst, (f) longitudinal cross-section of the OCT scan and (g) one-to-one correlation of OCT images and histopathology. The Figures are adapted with kind permission from [63, 64].

produced a significant difference between stroma, inflammation, Gleason 3, and Gleason 4 confirming the correlation of histopathology and OCT (Fig. 8). Precise matching of the images enabled differentiating the most histological tissues in the prostate by their unique pattern obtained by OCT. Recent advancements of micro-optical coherence tomography (μOCT) can generate depth-resolved tissue images with 1 μm resolution. Cellular-level contrast in prostate specimens was presented by the μOCT optical images, which helps in differentiating and diagnosing the pathologies. Specimens obtained from surgical resections were subjected μOCT imaging *ex vivo* and observed features correlated with the histological findings, suggesting that μOCT could resolve benign and neoplastic prostate associated cellular characteristics. μOCT can be implemented in a small-diameter probe which suggests that μOCT imaging may be used for needle-based virtual biopsy of the prostate [65].

Three pathologists carried out the pathological evaluation of full-field OCT (FF-OCT) diagnostic accuracy in the detection of cancer on prostate biopsy of 38 patients by determining sensitivity, specificity,

positive and negative prediction values. The observations of pathologists were on substantial agreement with over 72% accuracy. It was concluded that FF-OCT imaging of prostate biopsy would provide over 80% diagnostic accuracy with good reliability [66]. A customized tool was developed to validate OCT in the differentiation of prostate cancer by processing radical prostatectomy specimens to improve OCT pullback measurements. This is essential in the critical validation of OCT imaging studies by correlating histology and studying solid tissues such as lung, breast, ovary, kidney, and liver. Improvement in the efficacy of OCT in cancer detection and staging in solid organs was achieved [67]. Therefore, this non-invasive, real-time imaging approach has proven effective in detecting and differentiation cancerous prostate.

Table 3 Diagnostic summary.

Cancer types	**Types of OCT**	**Diagnostic summary**	**Reference**
Colorectal cancer	Integrated multimodal OCT and NIR fluorescence imaging system	OCT endoscopy helps visualize the microanatomy of the subsurface layer structures with microscopic detail and NIR fluorescence imaging can be used to identify the suspect lesions rapidly	[13]
	Multimodal FD-OCT with Raman spectroscopy	The multimodal optical approach discriminated between colonic adenocarcinoma and normal colon with 97% sensitivity and specificity	[14]
	Co-registered OCT and fluorescence molecular imaging (FMI) system	This system enables simultaneous imaging of tissue morphology and molecular information at high resolution over 2–3 mm field-of-view, and will have potential applications in small animal imaging and clinical imaging	[18]
Breast cancer	Handheld surgical OCT imaging probe	The *ex vivo* images were compared with standard post-operative histopathology to yield sensitivity of 91.7% [95% confidence interval (CI), 62.5%–100%] and specificity of 92.1% (95% CI, 78.4%–98%)	[20]
	Optical coherence microelastography (OCME)	OCT readily distinguishes mature stroma and tumour from adipose in tissue, microelastograms exhibit high contrast between tissues with similar optical backscattering properties. Together, OCME is shown to enable ready visualization of features such as ducts, lobules, microcysts, blood vessels, and arterioles and to identify invasive tumour through distinctive patterns	[25]
	Optical coherence elastography (OCE)	OCE imaging ensures much higher contrast between different tissue types in comparison with both structural OCT images (including PS-OCT) and conventionally used elastographic techniques	[26]
	FF-OCT and dynamic cell imaging (DCI)	FFOCT has been used to differentiate benign and malignant breast tissues and provides a platform for diagnostic decision making. Its sensitivity and specificity both are roughly over 90%. DCI is used to visualize tissues on a cellular scale with metabolic features coupled with the morphologic imaging of FFOCT	[27]
	PS-OCT	In the study, healthy fibro-adipose tissue, healthy stroma, and invasive ductal carcinoma can be differentiated with an accuracy of 89.4%	[28]

	SS-OCT	The SVM based automated volumetric analysis of normal and breast cancer tissue classifies the cancerous tissue with sensitivity, specificity, and accuracy of 91.56%, 93.86%, and 92.71% respectively	[29]
	OCT and OCM	The system enabled 4-μm axial resolution (OCT and OCM) with 14-μm (OCT) and 2-μm (OCM) transverse resolutions, respectively. OCT and OCM provide complimentary information about tissue microstructure, thus showing distinctive patterns for adipose tissue, fibrous stroma, breast lobules and ducts, cysts and micro-cysts, as well as in situ and invasive carcinomas	[30]
	OCT	The developed multi-level ensemble classifier attained the average sensitivity, specificity, accuracy and Mathew correlation coefficient is 0.954%, 0.93%, 94.35%, and 0.887% in classifying normal and cancerous breast tissue	[31]
		The *ex vivo* study with OCT showed significant difference in the hair structure before and after chemotherapy due to reduction of hair shaft calibre and increase of form factor in regrowing hair	[32]
	FF-OCT	Using FF-OCT images, two breast pathologists were able to distinguish normal/benign tissue from lesion with a sensitivity of 94% and 90%, and specificity of 75% and 79% respectively	[49]
Skin cancer	OCT and PS-OCT	OCT and PS-OCT analysis showed 79% to 94% sensitivity and 85% to 96% specificity in differentiating normal skin from non-melanoma skin cancer lesions	[33]
	SS-OCT	Among the classifiers, Linear SVM (LSVM) yielded the optimum result with an accuracy rate of 80.9%, specificity of 80.5% and sensitivity of 81.9% for BCC classification. With quadratic SVM (QSVM) an accuracy rate of 87.2%, specificity of 87.3% and sensitivity of 87% were obtained for SCC classifications. QSVM also provided satisfying results, 80.5% accuracy for BCC classification	[34]
		In the study, clinically identified melanoma to non-melanoma area showed a meaningful difference. Further, classification of sample using Gaussian SVM provided highest classification accuracy of 98% with other evaluation matrix	[36]
	Multi-beam OCT	This study showed that it is possible to distinguish between the different non melanoma skin cancers by using OCT	[35]
	Multi-beam-FD-SS OCT	Abrupt changes in architectures of the dermal and epidermal layers in the GCT lesion were observed. These architectural changes were not observed in healthy skin	[37]
	Vivosight OCT Scanner	The depth of superficial basal cell carcinoma (BCC) lesions (<1 mm) can be measured accurately using OCT. A low-strength OCT signal at the periphery of the cell nests seen in superficial and nodular BCC is identified as corresponding to cellular palisading. A weak inverse linear correlation (r^2=0.3) is found between the optical attenuation coefficient measured on OCT and the nuclear-cytoplasmic ratio (N/C) of cells determined from histology	[40]

		The specificity increased significantly from 28.6% by clinical assessment to 54.3% using dermoscopy and to 75.3% with the addition of OCT. The accuracy of diagnosis for all lesions increased from 65.8% with clinical evaluation to 76.2% following additional dermoscopy and to 87.4% with the addition of OCT	[42]
	OCT	OCT could identify superficial BCC and acute keratosis before treatment. Monitoring during imiquimod treatment revealed impaired image quality most likely caused by inflammation, crusting and ulceration	[41]
	PS-OCT	The SVM classifier achieved 95.4% sensitivity in the classification of basal cell carcinoma (BCC) from normal samples	[43]
	FD-OCT	Diagnostic performance of OCT did not depend on the lesion's anatomical location. Good OCT image quality was correlated with improved diagnostic performance, but diagnostic performance for lesions with mediocre image quality was still better than by clinical and dermoscopic examination	[44]
		FD-OCT with a new depiction for horizontal and vertical imaging modes offers additional information in the diagnosis of BCC, especially in nodular BCC, and enhances the possibility of the evaluation of morphologic tumour features	[45]
Brain cancer	CP-OCT	The diagnostic threshold of attenuation coefficient was 8.2 mm^{-1} for patients of all grades (sensitivity/specificity: 95.6%/81.3%, respectively) and 6.1 mm^{-1} for low-grade patients (sensitivity/specificity: 100%/100%, respectively)	[52]
		Visual assessment of CP OCT images enables tumorous and non-tumorous tissues is distinguished based on differentiation between tumorous tissue and white matter. The diagnostic accuracy for the same is 87–88%	[55]
	FF-OCT	FF-OCT captures slices of tissue samples at 1 μm axial and lateral resolution in 3D to a penetration depth of around 200 μm	[53]
	SS-OCT	The technique exhibited comparable 100% sensitivity and 40–50% greater specificity in detecting the cancer	[54]
Ovarian cancer	FD-PS OCT	Linear regression analysis showed that this parameter was positively correlated (R = 0.74) with collagen content, which was associated with the development of ovarian tissue malignancy. With 33 ovaries training dataset the logistic model produced 100% sensitivity and specificity whereas, model validation with new dataset showed 100% sensitivity and 83.3% specificity	[58]
	PS-OCT	A specificity of 100% and a sensitivity of 86% were achieved by using estimated scattering coefficient alone; and a specificity of 100% and a sensitivity of 43% were obtained by using phase retardation alone. However, a superior specificity of 100% and sensitivity of 100% were achieved if these two parameters were used together for classifying normal and malignant ovaries	[59]

Prostate cancer	Needle based OCT	This study will provide insight into the feasibility and tissue-specific characteristics of confocal laser endomicroscopy and optical coherence tomography for real-time optical analysis of prostate cancer	[63]
		OCT can reliably differentiate between fat, cystic, and regular atrophy and benign glands. In blind assessment of OCT images, the overall sensitivity and specificity for malignancy detection was 79% and 88% for Reviewer 1 and 88% and 81% for Reviewer 2	[64]
	μOCT	From the system, high-quality image data were obtained at a penetration depth up to 500 μm. This technique is capable of resolving many of the architectural and cellular features associated with benign and neoplastic prostate	[65]
	FF-OCT	FF-OCT of prostate biopsy cores may provide a diagnostic accuracy greater than 80%, with a good reliability and high negative predictive values.	[66]
Lung cancer	FD-OCT	Permeability coefficients showed statistically significant differences between benign lung granulomatosis and normal tissues	[72]
	PS-OCT	The sensitivity and specificity of using OCT in diagnosing different types of lung cancer were in the range of 80–100%	[73]

4.7 Lung Cancer

Lung cancer is the most common cause of cancer-related deaths in men and women around the globe. High-resolution imaging technology is required to have an insight into pathophysiology and diagnose lung cancer and other pulmonary related diseases. Currently, the two imaging techniques available are OCT and CLE. OCT can be used to detect malignant cells in the lung parenchyma, central airways, pleura, and lymph nodes. By evaluating the malignant area in airway walls using OCT, the treatment including airway remodelling is possible [68]. *In vivo* endoscopic OCT can be used to produce real-time cross-sectional images of living tissues [69]. Michel et al. [70] was the first to report the use of OCT to differentiate malignant endobronchial from normal endobronchial mucosa. OCT scans were obtained after the performance on both malignant and normal endobronchial mucosa. The whole procedure was completed in around 30 min. OCT scan of endobronchial mucosa displayed malignancy along with loss of microstructures and optical fractures of tissues. The diagnostic accuracy of OCT provided a sensitivity of 100% and specificity of 80%, 70% when considering layer thickness and the attenuation coefficient, respectively. Wessels et al. [71] presented that qualitative and quantitative OCT imaging can distinguish between benign and (pre)malignant vulvar tissue.

Wei et al. [72] evaluated the effects of diffusion of analyte mediated by ultrasound on the permeability of benign, normal, and malignant lung tissues *in vitro*. It was also used to determine effective sonophoretic (SP) delivery combined with optical clearing agents (OCAs) to distinguish between normal and diseased tissues. FD-OCT was used to determine the permeability coefficient of SP combined OCAs method. The result of permeability coefficients showed statistically significant differences between benign lung granulomatosis and normal tissues. Ultrasound mediated OCAs method combined with FD-OCT suggested a potential diagnosis and detection of microstructure change in human lung tissues. Hariri et al. [73] proved that OCT could not replace histopathology but could be used in place of biopsies to diagnose lung cancer. The sensitivity and specificity of using OCT in diagnosing different types of lung cancer were in the range of 80–100% (as represented in Figs. 1–3 of Ref. [73]). Biopsies must include enough tumour for the diagnosis with the advancement in personalized medicine. However, diagnosis may delay due to unplanned biopsy of tumour-associated fibrosis, also affecting the tumour yield. Differentiating tumour from tumour-associated fibrosis during biopsy could remarkably elevate tumour yield. Hariri et al. [74] demonstrated that PS-OCT could effectively be used to identify tumours from fibrosis taken from lung sample and thus can be used for *in vivo* intraprocedural tissue sampling or *ex vivo* rapid biopsy assessment to obtain increased tumour yield for the diagnosis of cancer.

Jain et al. [75] presented a study in which FF-OCT was used to produce high-resolution lung tissue images. It showed to have potential in identifying tumours from non-neoplastic lung tissue. Distinguishing features such as lung collapse and smoker's macrophages were also identified in the sample tissues. Another study conducted by d'Hooghe et al. [76] reported OCT-based imaging of airway walls layers both *in vivo* and *ex vivo*. It was an

accurate imaging technique for quantifying and identifying airway wall layers and has a potential airway remodelling in lung diseases. This intraoperative, non-invasive, and real-time imaging technique has the potential in detecting different types of lung cancer such as poorly differentiated carcinoma, squamous cell carcinoma and adenocarcinoma.

5 Conclusion

OCT is an effective and convenient tool for various bio-clinical fields, including the characterization and diagnosis of different diseases. The various studies indicate that the technique, when combined with other imaging modalities, show an enhanced effect. Simultaneous assessment of images in PS-OCT is more effective in a detailed understanding of the molecule orientation [10]. In this review, we discuss the importance of detection of several cancers. However, this technique can also be used in investigating other diseases. The integration of adaptive optics in OCT can image deeper regions in tissue by overcoming the wavefront distortion of the sample as well as optics used.

Cancer cell growth in the tissue causes variation in tissue features such as shape and size of microstructures, density, etc. And OCT is one such technique to identify such minute changes associated with tissue microstructures. However, they may fail to differentiate similar morphological structures, which in turn decreases the output accuracy. In this regard, the incorporation of a proper post-processing and quantitative analysis technique plays an important role in differentiating benign and malignant tissue with high classification accuracy [32, 34]. The quality of images obtained by OCT can be enriched by deducing the properties of the object numerically with signal processing. Further analysis will enhance the details obtained depending on the data quality. Signal processing ensures maximum use of the data available by decreasing the noise and confirming accurate image formation. It can be beneficial in reducing noise, improving resolution through deconvolution, reducing speckle, correcting for material dispersion and OCT system imperfections, and de-blurring the defocusing effects outside of the depth-of-field of the OCT instrument [48]. Later, different optical, textural features extracted from these pre-processed images are used in training the statistical algorithms to achieve tissue classification [32, 34].

6 Future prospects of OCT in oncological diagnosis and treatment

The use of OCT at every step in oncology appears to be very promising, which will bring a major change in medical practice in the best way in the future. Obtaining optical access to the tissue site is currently a major challenge, yet the use of OCT appears to greater potentials with higher resolutions than other techniques currently used in oncological imaging. Where conventional biopsy is not effective, OCT can be used for guided biopsy, in many situations, biopsy is associated with many complications, so we can play the role of OCT as a tissue specific differentiation guide. OCT is among the best techniques that can assist in intraoperative imaging of various kind of cancer and other disease in the operation room by providing specific and real-time feedback to surgeons during specialized and complex surgeries. OCT can be used to monitor tumour responses to various types of cancer treatments such as photodynamic therapy, radiotherapy, thermotherapy, cryotherapy, and chemotherapy and the tissue changes that occur in them. OCT in oncopathology will be presented with strong demonstrations, with an emphasis on *ex vivo* and *in vivo* cancer diagnosis applications, given the development and broad potential. Currently, the utility of this technology can be seen in the criteria-based market, given the availability of various commercial OCT imaging systems and OCT probes, OCT in the field of oncology appears to be full of immense potential which proves to be an important milestone.

Compliance with ethical standards

The cited reference papers have ethical clearance for conducting the experiments.

Disclosures

All authors declare that there is no conflict of interests in this paper.

Acknowledgments

We thank the Department of Science and Technology (DST), Government of India, for the financial support (project number: DST/INT/Thai/P-10/2019 and DST/INT/BLG/P-3/2019). The authors thank Manipal School of Life Sciences (MSLS), Manipal Academy of Higher Education (MAHE), Manipal, Karnataka, India for providing the infrastructure and facilities.

References

1. M. E. Brezinski, G. J. Tearney, B. E. Bouma, J. A. Izatt, M. R. Hee, E. A. Swanson, J. F. Southern, and F. G. Fujimoto, "Optical coherence tomography for optical biopsy: properties and demonstration of vascular pathology," Circulation 93(6), 1206–1213 (1996).

2. P. A. Valdés, D. W. Roberts, F. K. Lu, and A. Golby, "Optical technologies for intraoperative neurosurgical guidance," Neurosurgical Focus 40(3), E8 (2016).
3. W. Drexler, U. Morgner, F. X. Kärtner, C. Pitris, S. A. Boppart, X. D. Li, E. P. Ippen, and J. G. Fujimoto, "In vivo ultrahigh-resolution optical coherence tomography," Optics Letters 24(17), 1221–1223 (1999).
4. J. G. Fujimoto, M. E. Brezinski, G. J. Tearney, S. A. Boppart, B. Bouma, M. R. Hee, J. F. Southern, and E. A. Swanson, "Optical biopsy and imaging using optical coherence tomography," Nature Medicine 1(9), 970–972 (1995).
5. J. G. Fujimoto, C. Pitris, S. A. Boppart, and M. E. Brezinski, "Optical coherence tomography: an emerging technology for biomedical imaging and optical biopsy," Neoplasia 2(1-2), 9–25 (2000).
6. W. Drexler, J. G. Fujimoto, "State-of-the-art retinal optical coherence tomography," Progress in Retinal and Eye Research 27(1), 45–88 (2008).
7. T. Klein, R. Huber, "High-speed OCT light sources and systems," Biomedical Optics Express 8(2), 828–859 (2017).
8. J. F. de Boer, C. K. Hitzenberger, and Y. Yasuno, "Polarization sensitive optical coherence tomography - a review," Biomedical Optics Express 8(3), 1838–1873 (2017).
9. A. Dubois, L. Vabre, A. C. Boccara, and E. Beaurepaire, "High-resolution full-field optical coherence tomography with a Linnik microscope," Applied Optics 41(4), 805–812 (2002).
10. S. R. Chinn, E. A. Swanson, and J. G. Fujimoto, "Optical coherence tomography using a frequency-tunable optical source," Optics Letters 22(5), 340–342 (1997).
11. J. P. Kolb, T. Pfeiffer, M. Eibl, H. Hakert, and R. Huber, "High-resolution retinal swept source optical coherence tomography with an ultra-wideband Fourier-domain mode-locked laser at MHz A-scan rates," Biomedical Optics Express 9(1), 120–130 (2017).
12. S. Yun, G. Tearney, J. de Boer, N. Iftimia, and B. Bouma, "High-speed optical frequency-domain imaging," Optics Express 11(22), 2953–2963 (2003).
13. Y. Li, Z. Zhu, J. J. Chen, J. C. Jing, C. H. Sun, S. Kim, P. S. Chung, and Z. Chen, "Multimodal endoscopy for colorectal cancer detection by optical coherence tomography and near-infrared fluorescence imaging," Biomedical Optics Express 10(5), 2419–2429 (2019).
14. P. C. Ashok, B. B. Praveen, N. Bellini, A. Riches, K. Dholakia, and C. S. Herrington, "Multi-modal approach using Raman spectroscopy and optical coherence tomography for the discrimination of colonic adenocarcinoma from normal colon," Biomedical Optics Express 4(10), 2179–2186 (2013).
15. N. Stone, C. Kendall, J. Smith, P. Crow, and H. Barr, "Raman spectroscopy for identification of epithelial cancers," Faraday Discuss 126, 141–157 (2004).
16. N. Krstajić, C. T. Brown, K. Dholakia, and M. E. Giardini, "Tissue surface as the reference arm in Fourier domain optical coherence tomography," Journal of Biomedical Optics 17(7), 071305 (2012).
17. D. E. Fleischer, B. F. Overholt, V. K. Sharma, A. Reymunde, M. B. Kimmey, R. Chuttani, K. J. Chang, R. Muthasamy, C. J. Lightdale, N. Santiago, and D. K. Pleskow, "Endoscopic radiofrequency ablation for Barrett's esophagus: 5-year outcomes from a prospective multicenter trial," Endoscopy 42(10), 781–789 (2010).
18. S. Yuan, C. A. Roney, J. Wierwille, C. W. Chen, B. Xu, G. Griffiths, J. Jiang, H. Ma, A. Cable, R. M. Summers, and Y. Chen, "Co-registered optical coherence tomography and fluorescence molecular imaging for simultaneous morphological and molecular imaging," Physics in Medicine & Biology 55(1), 191 (2010).
19. E. S. Hwang, D. Y. Lichtensztajn, S. L. Gomez, B. Fowble, and C. A. Clarke, "Survival after lumpectomy and mastectomy for early stage invasive breast cancer: the effect of age and hormone receptor status," Cancer 119(7), 1402–1411 (2013).
20. S. J. Erickson-Bhatt, R. M. Nolan, N. D. Shemonski, S. G. Adie, J. Putney, D. Darga, D. T. McCormick, A. J. Cittadine, A. M. Zysk, M. Marjanovic, and E. J. Chaney, "Real-time imaging of the resection bed using a handheld probe to reduce incidence of microscopic positive margins in cancer surgery," Cancer Research 75(18), 3706–3712 (2015).
21. J. Wang, Y. Xu, and S. A. Boppart, "Review of optical coherence tomography in oncology," Journal of Biomedical Optics 22(12), 121711 (2017).
22. K. H. Allison, "Molecular pathology of breast cancer: what a pathologist needs to know," American Journal of Clinical pathology 138(6), 770–780 (2012).
23. O. A. Catalano, G. L. Horn, A. Signore, C. Iannace, M. Lepore, M. Vangel, A. Luongo, M. Catalano, C. Lehman, M. Salvatore, and A. Soricelli, "PET/MR in invasive ductal breast cancer: correlation between imaging markers and histological phenotype," British Journal of Cancer 116(7), 893–902 (2017).
24. B. F. Kennedy, S. H. Koh, R. A. McLaughlin, K. M. Kennedy, P. R. Munro, and D. D. Sampson, "Strain estimation in phase-sensitive optical coherence elastography," Biomedical Optics Express 3(8), 1865–1879 (2012).
25. B. F. Kennedy, R. A. McLaughlin, K. M. Kennedy, L. Chin, P. Wijesinghe, A. Curatolo, A. Tien, M. Ronald, B. Latham, C. M. Saunders, and D. D. Sampson, "Investigation of optical coherence microelastography as a method to visualize cancers in human breast tissue," Cancer Research 75(16), 3236–3245 (2015).
26. E. V. Gubarkova, A. A. Sovetsky, V. Y. Zaitsev, A. L. Matveyev, D. A. Vorontsov, M. A. Sirotkina, L. A. Matveev, A. A. Plekhanov, N. P. Pavlova, S. S. Kuznetsov, and A. Y. Vorontsov, "OCT-elastography-based optical biopsy for

breast cancer delineation and express assessment of morphological/molecular subtypes," Biomedical Optics Express 10(5), 2244–2263 (2019).
27. H. Yang, S. Zhang, P. Liu, L. Cheng, F. Tong, H. Liu, S. Wang, M. Liu, C. Wang, Y. Peng, and F. Xie "Use of high-resolution full-field optical coherence tomography and dynamic cell imaging for rapid intraoperative diagnosis during breast cancer surgery," Cancer 126, 3847–3856 (2020).
28. J. Wang, Y. Xu, K. J. Mesa, F. A. South, E. J. Chaney, D. R. Spillman, R. Barkalifa, M. Marjanovic, P. S. Carney, A. M. Higham, and Z. G. Liu, "Complementary use of polarization-sensitive and standard OCT metrics for enhanced intraoperative differentiation of breast cancer," Biomedical Optics Express 9(12), 6519–6528 (2018).
29. A. Butola, A. Ahmad, V. Dubey, V. Srivastava, D. Qaiser, A. Srivastava, P. Senthilkumaran, and D. S. Mehta, "Volumetric analysis of breast cancer tissues using machine learning and swept-source optical coherence tomography," Applied Optics 58(5), A135–A141 (2019).
30. C. Zhou, D. W. Cohen, Y. Wang, H. C. Lee, A. E. Mondelblatt, T. H. Tsai, A. D. Aguirre, J. G. Fujimoto, and J. L. Connolly, "Integrated optical coherence tomography and microscopy for ex vivo multiscale evaluation of human breast tissues," Cancer Research 70(24), 10071–10079 (2010).
31. K. Dubey, N. Singla, A. Butola, A. Lathe, D. Quaiser, A. Srivastava, D.S. Mehta, and V. Srivastava, "Ensemble classifier for improve diagnosis of the breast cancer using optical coherence tomography and machine learning," Laser Physics Letters 16(2), 025602 (2019).
32. J. Lindner, K. Hillmann, U. Blume-Peytavi, J. Lademann, A. Lux, A. Stroux, A. Schneider, and N. Garcia Bartels, "Hair shaft abnormalities after chemotherapy and tamoxifen therapy in patients with breast cancer evaluated by optical coherence tomography," British Journal of Dermatology 167(6), 1272–1278 (2012).
33. M. Mogensen, T. M. Joergensen, B. M. Nürnberg, H. A. Morsy, J. B. Thomsen, L. Thrane, and G. B. Jemec, "Assessment of optical coherence tomography imaging in the diagnosis of non-melanoma skin cancer and benign lesions versus normal skin: observer-blinded evaluation by dermatologists and pathologists," Dermatologic Surgery 35(6), 965–972 (2009).
34. S. Adabi, M. Hosseinzadeh, S. Noei, S. Conforto, S. Daveluy, A. Clayton, D. Mehregan, and M. Nasiriavanaki, "Universal in vivo textural model for human skin based on optical coherence tomograms," Scientific Reports 7(1), 17912 (2017).
35. S. Batz, C. Wahrlich, A. Alawi, M. Ulrich, and J. Lademann, "Differentiation of different nonmelanoma skin cancer types using OCT," Skin Pharmacology and Physiology 31(6), 238–245 (2018).
36. Z. Turani, E. Fatemizadeh, T. Blumetti, S. Daveluy, A. F. Moraes, W. Chen, D. Mehregan, P. E. Andersen, and M. Nasiriavanaki, "Optical radiomic signatures derived from optical coherence tomography images improve identification of melanoma," Cancer Research 79(8), 2021–2030 (2019).
37. D. Tes, A. Aber, M. Zafar, L. Horton, A. Fotouhi, Q. Xu, A. Moiin, A. D. Thompson, T. C. Moraes Pinto Blumetti, S. Daveluy, and W. Chen, "Granular cell tumor imaging using optical coherence tomography," Biomedical Engineering and Computational Biology 9, 1179597218790250 (2018).
38. A. L. Agero, K. J. Busam, C. Benvenuto-Andrade, A. Scope, M. Gill, A. A Marghoob, S. González, and A. C. Halpern, "Reflectance confocal microscopy of pigmented basal cell carcinoma," Journal of the American Academy of Dermatology 54(4), 638–643 (2006).
39. S. Seidenari, F. Arginelli, S. Bassoli, J. Cautela, A.M. Cesinaro, M. Guanti, D. Guardoli, C. Magnoni, M. Manfredini, G. Ponti, and K. König, "Diagnosis of BCC by multiphoton laser tomography," Skin Research and Technology 19(1), e297–e304 (2013).
40. A. J. Coleman, T. J. Richardson, G. Orchard, A. Uddin, M. J. Choi, and K. E. Lacy, "Histological correlates of optical coherence tomography in non-melanoma skin cancer," Skin Research and Technology 19(1), e10–e19 (2013).
41. C. A. Banzhaf, L. Themstrup, H. C. Ring, M. Mogensen, and G. B. Jemec, "Optical coherence tomography imaging of non-melanoma skin cancer undergoing imiquimod therapy," Skin Research and Technology 20(2), 170–176 (2014).
42. M. Ulrich, T. von Braunmuehl, H. Kurzen, T. Dirschka, C. Kellner, E. Sattler, C. Berking, J. Welzel, and U. Reinhold, "The sensitivity and specificity of optical coherence tomography for the assisted diagnosis of nonpigmented basal cell carcinoma: an observational study," British Journal of Dermatology 173(2), 428–435 (2015).
43. T. Marvdashti, L. Duan, S. Z. Aasi, J. Y. Tang, and A. K. Bowden, "Classification of basal cell carcinoma in human skin using machine learning and quantitative features captured by polarization sensitive optical coherence tomography," Biomedical Optics Express 7(9), 3721–3735 (2016).
44. J. Holmes, T. von Braunmühl, C. Berking, E. Sattler, M. Ulrich, U. Reinhold, H. Kurzen, T. Dirschka, C. Kellner, S. Schuh, and J. Welzel, "Optical coherence tomography of basal cell carcinoma: influence of location, subtype, observer variability and image quality on diagnostic performance," British Journal of Dermatology 178(5), 1102–1110 (2018).
45. T. von Braunmühl, D. Hartmann, J. K. Tietze, D. Cekovic, C. Kunte, T. Ruzicka, C. Berking, and E. C. Sattler, "Morphologic features of basal cell carcinoma using the en-face mode in frequency domain optical coherence tomography," Journal of the European Academy of Dermatology and Venereology 30(11), 1919–1925 (2016).

46. J. Gogas, C. Markopoulos, E. Kouskos, H. Gogas, D. Mantas, Z. Antonopoulou, and K. Kontzoglou, "Granular cell tumor of the breast: a rare lesion resembling breast cancer," European Journal of Gynaecological Oncology 23(4), 333–334 (2002).
47. M. Lacroix, D. Abi-Said, D. R. Fourney, Z. L. Gokaslan, W. Shi, F. DeMonte, F. F. Lang, I. E. McCutcheon, S. J. Hassenbusch, E. Holland, and K. Hess, "A multivariate analysis of 416 patients with glioblastoma multiforme: prognosis, extent of resection, and survival," Journal of Neurosurgery 95(2), 190–198 (2001).
48. N. Sanai, M. Y. Polley, M. W. McDermott, A. T. Parsa, and M. S. Berger, "An extent of resection threshold for newly diagnosed glioblastomas," Journal of Neurosurgery 115(1), 3–8 (2011).
49. O. Assayag, M. Antoine, B. Sigal-Zafrani, M. Riben, F. Harms, A. Burcheri, K. Grieve, E. Dalimier, B. Le Conte de Poly, and C. Boccara, "Large field, high resolution full-field optical coherence tomography: a pre-clinical study of human breast tissue and cancer assessment," Technology in Cancer Research & Treatment 13(5), 455–468 (2014).
50. T. Alice, N. Georges, "Medulloblastoma: optimizing care with a multidisciplinary approach," Journal of Multidisciplinary Healthcare 12, 335–347 (2019).
51. F. J. van der Meer, D. J. Faber, D. M. Baraznji Sassoon, M. C. Aalders, G. Pasterkamp, and T. G. van Leeuwen, "Localized measurement of optical attenuation coefficients of atherosclerotic plaque constituents by quantitative optical coherence tomography," IEEE Transactions on Medical Imaging 24(10), 1369–1376 (2005).
52. K. S. Yashin, E. B. Kiseleva, A. A. Moiseev, S. S. Kuznetsov, L. B. Timofeeva, N. P. Pavlova, G. V. Gelikonov, I. A. Medyanik, L. Y. Kravets, E. V. Zagaynova, and N. D. Gladkova, "Quantitative nontumorous and tumorous human brain tissue assessment using microstructural co- and cross-polarized optical coherence tomography," Scientific Reports 9(1), 2024 (2019).
53. O. Assayag, K. Grieve, B. Devaux, F. Harms, J. Pallud, F. Chretien, C. Boccara, and P. Varlet, "Imaging of non-tumorous and tumorous human brain tissues with full-field optical coherence tomography," NeuroImage: Clinical 2, 549–557 (2013).
54. C. Kut, K. L. Chaichana, J. Xi, S. M. Raza, X. Ye, E. R. McVeigh, F. J. Rodriguez, A. Quiñones-Hinojosa, and X. Li, "Detection of human brain cancer infiltration ex vivo and in vivo using quantitative optical coherence tomography," Science Translational Medicine 7(292), 292ra100-292ra100 (2015).
55. K. S. Yashin, E. B. Kiseleva, E. V. Gubarkova, A. A. Moiseev, S. S. Kuznetsov, P. A. Shilyagin, G. V. Gelikonov, I. A. Medyanik, L. Y. Kravets, A. A. Potapov, and E. V. Zagaynova, "Cross-polarization optical coherence tomography for brain tumor imaging," Frontiers in Oncology 9, 201 (2019).
56. T. R. Rebbeck, H. T. Lynch, S. L. Neuhausen, S. A. Narod, L. Van't Veer, J. E. Garber, G. Evans, C. Isaacs, M. B. Daly, E. Matloff, and O. I . Olopade, "Prophylactic oophorectomy in carriers of BRCA1 or BRCA2 mutations," New England Journal of Medicine 346(21), 1616–1622 (2002).
57. C. St-Pierre, W. J. Madore, E. De Montigny, D. Trudel, C. Boudoux, N. Godbout, A. M. Mes-Masson, K. Rahimi, and F. Leblond, "Dimension reduction technique using a multilayered descriptor for high-precision classification of ovarian cancer tissue using optical coherence tomography: a feasibility study," Journal of Medical Imaging 4(4), 041306 (2017).
58. T. Wang, Y. Yang, and Q. Zhu, "A three-parameter logistic model to characterize ovarian tissue using polarization-sensitive optical coherence tomography," Biomedical Optics Express 4(5), 772–777 (2013).
59. Y. Yang, T. Wang, X. Wang, M. Sanders, M. Brewer, and Q. Zhu, "Quantitative analysis of estimated scattering coefficient and phase retardation for ovarian tissue characterization," Biomedical Optics Express, 3(7) 1548–1556 (2012).
60. D. L. Marks, T. S. Ralston, and S. A. Boppart "Data analysis and signal postprocessing for Optical Coherence Tomography," In Optical Coherence Tomography, W. Drexler, J. G. Fujimoto (eds.), Springer, Berlin, Heidelberg, 405–426 (2008).
61. J. Liu, Y. Li, D. Yang, C. Yang, and L. Mao, "Current state of biomarkers for the diagnosis and assessment of treatment efficacy of prostate cancer," Discovery Medicine 27(150), 235–243 (2019).
62. J. Wang, J. Ni, J. Beretov, J. Thompson, P. Graham, and Y. Li, "Exosomal microRNAs as liquid biopsy biomarkers in prostate cancer," Critical Reviews in Oncology/Hematology 145, 102860 (2020).
63. A. Swaan, C. K. Mannaerts, M. J. Scheltema, J. A. Nieuwenhuijzen, C. D. Savci-Heijink, J. J. de la Rosette, R. J. Van Moorselaar, T. G. Van Leeuwen, T. M. De Reijke, and D. M. De Bruin, "Confocal laser endomicroscopy and optical coherence tomography for the diagnosis of prostate cancer: a needle-based, in vivo feasibility study protocol (IDEAL phase 2A)," JMIR Research Protocols 7(5), e132 (2018).
64. B. G. Muller, R. van Kollenburg, A. Swaan, E. Zwartkruis, M. J. Brandt, L. S. Wilk, M. Almasian, A. W. Schreurs, D. J. Faber, L. R. Rozendaal, and A. N. Vis, "Needle-based optical coherence tomography for the detection of prostate cancer: a visual and quantitative analysis in 20 patients," Journal of Biomedical Optics 23(8), 086001 (2018).
65. J. A. Gardecki, K. Singh, C. L. Wu, and G. J. Tearney, "Imaging the human prostate gland using 1-μm-resolution optical coherence tomography," Archives of Pathology & Laboratory Medicine 143(3), 314–318 (2019)
66. J. Lopater, P. Colin, F. Beuvon, M. Sibony, E. Dalimier, F. Cornud, and N. B. Delongchamps, "Real-time cancer diagnosis during prostate biopsy: ex vivo evaluation of full-field optical coherence tomography (FFOCT) imaging on biopsy cores," World Journal of Urology 34(2), 237–243 (2016).

67. B. G. Muller, A. Swaan, D. M. de Bruin, W. van den Bos, A. W. Schreurs, D. J. Faber, E. C. Zwartkruis, L. Rozendaal, A. N. Vis, J. A. Nieuwenhuijzen, and R. J. van Moorselaar, "Customized tool for the validation of optical coherence tomography in differentiation of prostate cancer," Technology in Cancer Research & Treatment 16(1), 57–65 (2017).
68. A. Goorsenberg, K. A. Kalverda, J. Annema, and P. Bonta, "Advances in optical coherence tomography and confocal laser endomicroscopy in pulmonary diseases," Respiration 99(3), 190–205 (2020).
69. A. M. Sergeev, V. M. Gelikonov, G. V. Gelikonov, F. I. Feldchtein, R. V. Kuranov, N. D. Gladkova, N. M. Shakhova, L. B. Snopova, A. V. Shakhov, I. A. Kuznetzova, A. N. Denisenko, V. V. Pochinko, Yu. P. Chumakov, and O. S. Streltzova, "In vivo endoscopic OCT imaging of precancer and cancer states of human mucosa," Optics Express 1(13), 432–440 (1997).
70. R. G. Michel, G. T. Kinasewitz, K. M. Fung, and J. I. Keddissi, "Optical coherence tomography as an adjunct to flexible bronchoscopy in the diagnosis of lung cancer: a pilot study," Chest 138(4), 984–988 (2010).
71. R. Wessels, M. van Beurden, D. M. de Bruin, D. J. Faber, A. D. Vincent, J. Sanders, T. G. Van Leeuwen, and T. J. Ruers, "The value of optical coherence tomography in determining surgical margins in squamous cell carcinoma of the vulva: a single-center prospective study," International Journal of Gynecologic Cancer 25(1), 112–118 (2015).
72. H. Wei, G. Wu, Z. Guo, H. Yang, Y. He, S. Xie, and X. Guo, "Assessment of the effects of ultrasound-mediated glucose on permeability of normal, benign, and cancerous human lung tissues with the Fourier-domain optical coherence tomography," Journal of Biomedical Optics 17(11), 116006 (2012).
73. L. P. Hariri, M. Mino-Kenudson, M. Lanuti, A. J. Miller, E. J. Mark, and M. J. Suter, "Diagnosing lung carcinomas with optical coherence tomography," Annals of the American Thoracic Society 12(2), 193–201 (2015).
74. L. P. Hariri, D. C. Adams, M. B. Applegate, A. J. Miller, B. W. Roop, M. Villiger, B. E. Bouma, and M. J. Suter, "Distinguishing tumor from associated fibrosis to increase diagnostic biopsy yield with polarization-sensitive optical coherence tomography," Clinical Cancer Research 25(17), 5242–5249 (2019).
75. M. Jain, N. Narula, B. Salamoon, M. M. Shevchuk, A. Aggarwal, N. Altorki, B. Stiles, C. Boccara, and S. Mukherjee, "Full-field optical coherence tomography for the analysis of fresh unstained human lobectomy specimens," Journal of Pathology Informatics 4 (2013).
76. J. N. d'Hooghe, A. W. Goorsenberg, D. M. de Bruin, J. Roelofs, J. T. Annema, and P. I. Bonta, "Optical coherence tomography for identification and quantification of human airway wall layers," PloS ONE 12(10) e0184145 (2017).